2021 20th International Conference on Advanced Robotics (ICAR)
December 6-10, 2021. Ljubljana, Slovenia

Comparative Quantitative Analysis of Robotic Ultrasound Image Calibration Methods

Ruixuan Li, Yuyu Cai, Kenan Niu and Emmanuel Vander Poorten

Abstract— **Ultrasound (US) calibration is an important step in robotic 3D US reconstruction. It determines the spatial transformation from the tracking sensor frame to the US image frame. Up to now, many free-hand calibration methods have been developed. Some of them were applied in robotic systems. However, there is no comparative analysis for those employed methods in the robotic US system. Moreover, the required robotic scanning trajectory was normally unclear in previous work. Therefore, in this paper, we provided a comparative analysis of three popular US image calibration methods, namely cross-wire phantom, sphere phantom and Z phantom. Meanwhile, we attempted to provide concrete examples of using three phantoms to establish automatic robotic calibration frameworks. Demonstrated on a KUKA lightweight robot attached with a 2D US probe, different aspects were assessed to show the calibration performance and 3D US reconstruction accuracy. With the proposed robotic calibration frameworks, the total time of entire calibration procedure was shortened within 3 minutes for all three phantoms. The reconstruction results showed that the RMSE were less than 1.6 mm. The proposed automatic robotic US image calibration frameworks together with their quantitative analyses provide a foundation for further development and optimization. It could potentially facilitate the development of robotic US system.**

Keywords: robotic ultrasound calibration, 3D US reconstruction, position control, calibration phantom

I. INTRODUCTION

Ultrasound (US) is an appealing medical imaging modality that allows visualizing the anatomical structures underlying the skin. Thanks to its low cost, real-time imaging capability and non-radiative nature, 3D ultrasound reconstruction is widely used in different clinical applications ranging from interventional cardiology [1] to orthopedic surgery [2], [3].

In recent years, robotic 3D US reconstruction is extensively applied for intraoperative guidance to reduce the clinician's workload [4], [5]. However, the accuracy of US reconstruction is severely influenced by the quality of US image calibration [6]. An incorrect US image calibration can lead to severe 3D volume distortion [7]. Therefore, it is important to have a reliable, easy-to-follow and accurate US image calibration procedure for the robotic US system.

Several methods are applied in robotic systems [8]–[10] or free-hand US systems [11] for US image calibration. Huang *et al.* devised a robotic calibration method with a custom designed ball-shaped phantom and achieved a 0.8 mm average error [8]. Based on the known phantom geometry, the calibration parameters were estimated with robotic 3D translational motion. However, this method was restricted to the translation scanning since rotational parameters were not taken into account in calibration. This procedure could not be applied in general US scanning to cover the patient anatomy from all angles of view. Aalamifar *et al.* designed an active echo phantom to transmit and receive US signals to a 2D US probe for image calibration [9]. The reported precision ranged from 1.67 to 3.20 mm with the robotic system. Without using an external tracking system, this approach designed a complex scanning trajectory to align the probe with the active echo phantom. It led to a time consuming calibration process that took 15 to 35 min. Jiang *et al.* proposed a robotic US calibration with the robot's kinematic model and the specifications from the US probe manufacturer [10]. However, it is not always accessible to obtain such information from manufacturer. Moreover, the on-site US image calibration is necessary to enable the high accuracy. Furthermore, a number of calibration phantoms, such as cross-wire phantom, sphere phantom and Z phantom, were widely used in free-hand US system and achieved mean precision ranged from 0.44 to 1.54 mm [11]. After integrating with the optical tracking system, the US system could interact with the robot arm and realize a fully automatic calibration procedure. Nevertheless, these applications were somewhat limited by the complex US scanning trajectories and the multifarious data process. Moreover, robotic scanning trajectories for different calibration methods, considered as important practical details, are normally unclear in previous work.

This paper presents a quantitative comparison of robotic US image calibration on three popular US image calibration methods. Three fully automatic robotic US image calibration frameworks for these three methods were developed. In this context, different aspects were investigated and analyzed. We hope the work of this paper can have a certain use for reference in the future study to facilitate the development of automatic robotic US system.

II. METHOD

In this section, the comparison of included calibration methods will be introduced from four aspects: calibration algorithms, phantoms design, US image processing and robotic scanning trajectories.

R. Li, Y. Cai, K. Niu and E. Vander Poorten are with the Department of Mechanical Engineering, KU Leuven, Belgium (email: kenan.niu@kuleuven.be)

This project has received funding from the European Union's Horizon 2020 research and innovation programme under grant agreement No. 101016985 and Flemish Research Foundation (FWO) under grant agreement NO. G0A1420N.

A. Experimental setup

The robotic US system consisted of a lightweight robot (KUKA Robot LWR, Augsburg, Germany) with ±0.05 mm repeatability, a 7.5 MHz linear US probe with US device (Sonosite, FUJIFILM, USA) and an optical tracking system (FusionTrack 500, Atracsys, Switzerland) with 0.09 mm accuracy. Fig.1 illustrates the experimental setup and relevant frames in the robotic US system. A custom designed US probe housing was mounted at robot end effector with an optical marker. The optical tracking system tracked US probe pose in 6 degrees of freedom (DoF) with respect to its own origin, termed optical tracking frame. Meanwhile, corresponding US images were recorded as 640×480 pixels by a frame grabber (Epiphan Systems Inc. Palo Alto, Canada) at 30 Hz. These calibration phantoms were immersed in water tank and assembled with optical marker to record the poses in optical tracking frame. In addition, a PC workstation (Intel i7, CPU @2.6 GHz, 64G RAM) was used for data acquisition and processing. To ensure real time robot control, the Open Robot Control Middleware (Orocos) was employed and run at 1 kHz. Besides, eTasl (expressiongraph-based Task Specification Language), a constraint based task specification was utilized for robot position control [12].

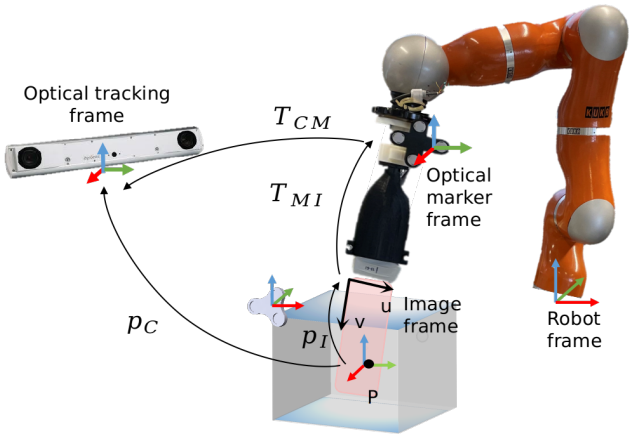

Fig. 1. Experimental setup and relevant transformations used in robotic US image calibration. The notation T_{BA} is used to denote transformation from coordinate system A to B.

B. Calibration algorithms

The aim of US image calibration is to determine the 3D spatial transformation (T_{MI}) from the image frame (I) to the optical marker frame (M) by using the customized phantom with specific geometries. In the optical tracking frame (C), T_{CM} is the transformation matrix from optical marker frame to the optical tracking frame. The pixels (u,v) in ultrasound image is presented as $p_I = [u,v,0,1]^T$. It can be converted to point clouds p_C in the optical tracking coordinates through Eq.1.

$$\begin{bmatrix} x \\ y \\ z \\ 1 \end{bmatrix} = T_{CM} \cdot T_{MI} \cdot \begin{bmatrix} s_u u \\ s_v v \\ 0 \\ 1 \end{bmatrix} \tag{1}$$

where u,v denote the column and row pixel indexes. s_u and s_v are column and row scalars in scaling matrix T_s, mapping the pixel distance to physical distance of the 2D US image, respectively. The transformation matrix (T_{MI}) and scaling factor matrix (T_s) are the calculated matrices through calibration procedure. They can be computed by minimizing the following equation with least squares method, where T_{CM}, p_{Ci} and p_{Ii} are known and can be measured.

$$f = \min \sum_{i=1}^{n} | \, T_{CM} \cdot T_{MI} \cdot T_s \cdot p_{Ii} - p_{Ci} \, | \tag{2}$$

C. Phantom design

Three involved phantoms were redesigned to fit the requirements of robotic US image calibration procedure.

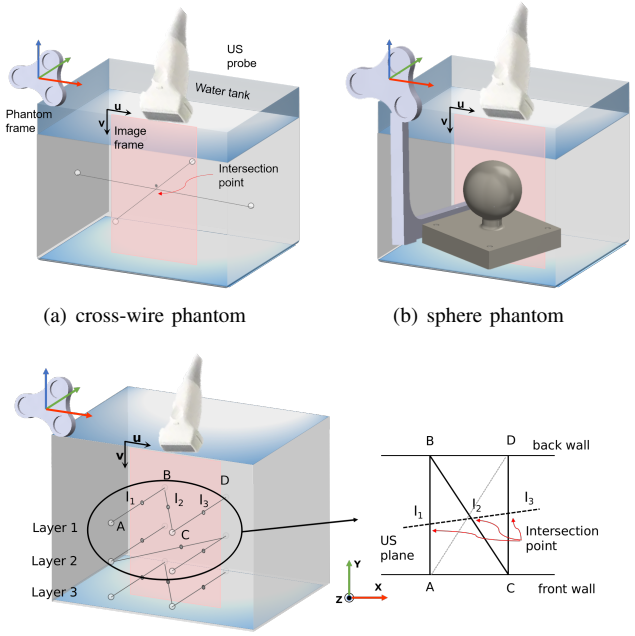

(a) cross-wire phantom

(b) sphere phantom

(c) Z phantom and top view of "Z" shaped wires

Fig. 2. Illustrations of three calibration phantoms. An optical marker is attached at each phantom to obtain the pose in optical tracking frame.

1) cross-wire phantom: The cross-wire phantom was categorized as a single point phantom [11]. It was made of two crossing nylon wires and immersed in a $150 \times 120 \times 40$ mm plastic box shown in Fig. 2 (a). The holes on the phantom wall were made by laser cutting to attach wires. During calibration, the cross point of two crossing wires needed to be viewed in the collected US images and identified in the latter image processing as p_{Ii}. To make US image acquisition step automatic for robotic calibration, an optical marker was attached at phantom wall. According to the designed geometrical parameters, the actual location of the cross point could be measured by the attached optical marker as p_{Ci}. Subsequently, the calibration matrix could be calculated by using Eq. 2.

2) sphere phantom: The sphere phantom was a variation of the cross-wire phantom. In this paper, a sphere phantom with 30 mm diameter was employed shown in Fig. 2 (b). The

diameter of the sphere was set to be able to capture a full contour of the phantom by using the linear US probe. The 3D printed sphere was assembled at a $50 \times 50 \times 10$ mm base and immersed in water. Besides, an optical marker was mounted at the sphere phantom base. The advantage of sphere shape phantom was the simplified image segmentation process due to the sphere appeared as a circle in the B-scans. The center of the sphere acted as the virtual target point p_{Ii} to replace the cross point in image frame. Meanwhile, the pose of the sphere center p_{Ci} was measured in optical tracking frame by the attached optical marker. The estimation of calibration matrix and scaling factors took place through Eq. 2 similar as the cross-wire phantom.

3) Z phantom: The Z phantom was made of three layers "Z" shaped crossing nylon wires. The size of phantom was $200 \times 100 \times 100$ mm. The distance between each layer was 10 mm, while the distance between point A and C was 20 mm, shown in Fig. 2 (c). The dimensions of "Z" shaped wires should within the US imaging area to ensure all points visible in US images. On the phantom wall, several holes were made by laser cutting as the predefined locations. With an attached optical marker and the designed geometrical parameters, the position of each hole could be located in the optical tracking frame. Thus, the Z coordinate of each layer in the optical tracking frame is constant, termed z^C. During scanning, each layer were intersected with the US image plane, displayed as three visible horizontal co-linear target points (I_1, I_2, I_3), shown in Fig. 2 (c). Based on similar triangles theorem [13], the position of the middle point in optical tracking frame can be determined by the two side points, by the following equation:

$$\begin{aligned} x^C_{I_2} &= x^C_B + \alpha \cdot (x^C_C - x^C_B) \\ y^C_{I_2} &= y^C_B + \alpha \cdot (y^C_C - y^C_B) \end{aligned} \tag{3}$$

where $[x^C_B, y^C_B, z^C_B]$ is the position of point B in optical tracking frame. The same notions are applied to the point I_2 and point C. The coefficient α is determined by the distance from I_2 to I_1 and I_3 in the image frame as follow:

$$\alpha = \frac{I_1 - I_2}{I_1 - I_3} = \frac{\sqrt{(u_{I_1} - u_{I_2})^2 + (v_{I_1} - v_{I_2})^2}}{\sqrt{(u_{I_1} - u_{I_3})^2 + (v_{I_1} - v_{I_3})^2}} \tag{4}$$

Then, the calibration parameters, T_{MI} and T_s, can be found by minimizing Eq. 2 with $p_C = [x^C_{I_2}, y^C_{I_2}, z^C_{I_2}, 1]^T$ and $p_I = [u_{I_2}, v_{I_2}, 0, 1]^T$.

D. Image processing

Based on geometry features of each phantom, different automatic image processing pipelines were developed to segment the target point p_I in US images. Fig. 3 illustrates the workflow of automatic US image segmentation and feature extraction. Firstly, the image enhancements were applied to raw US images for noise reduction and generated binary images. This processing consisted of Gussian filter, thresholding and morphological operator (closing) to remove small outliers and filling in the holes. Subsequently, the canny edge detection algorithm was applied to the binary image and segmented the contour of objectives. Dependent on the extracted objective features, different steps were implemented to recognize the required target point for calibration computation.

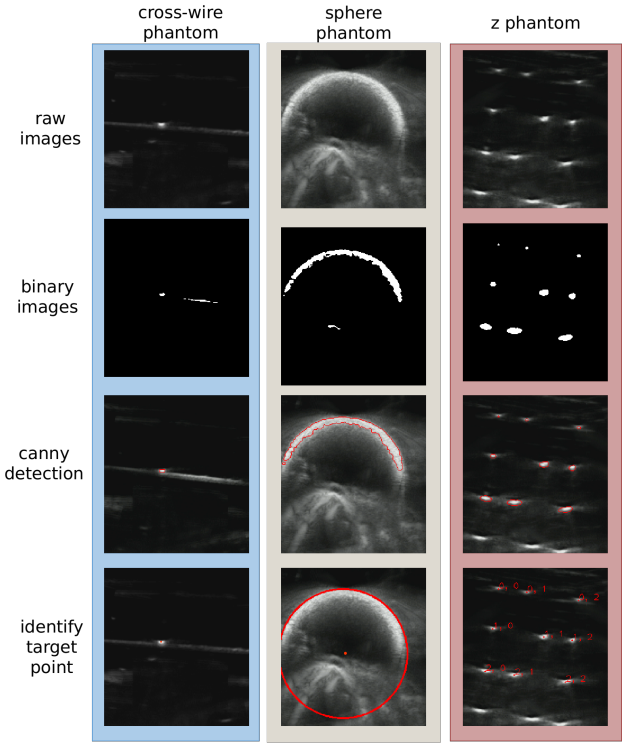

Fig. 3. The workflows to identify the target points in 2D images frame for cross-wire, sphere and Z phantoms

For the cross-wire phantom, the center of segmented point was scanned from the intersecting point in phantom as the target point p_I. For the sphere phantom, the sphere upper contour was extracted from the image [14]. Subsequently, the center of the sphere was estimated by fitting the circle to the contour with a least square optimization. The estimated center of the circle was used as target point to estimate the transformation matrices in Eq. 2. For Z phantom, there were 9 points in region of interest which were composed of 3 layers of "Z" shaped wires. Then, the points were sorted as three rows according to the vertical position, and the middle point of each row was selected as target points p_I in Eq. 3 for calibration calculations. To shorten the computation process, all of the image processes were optimized with Numba featuring with Compute Unified Device Architecture (CUDA) in python script.

E. Robotic scanning trajectories

The geometry features are different from phantoms. Due to that fact, the robotic scanning trajectory varies. This subsection introduces three examples for robotic scanning in three involved phantoms. The automatic robotic scanning consisted of two parts: camera-to-robot calibration and US calibration scanning.

In camera-to-robot calibration, the US probe was moved to predefined target points in robot frame by position control. The instantaneous marker position was recorded in the optical tracking frame as well as in the robot frame. Then, the camera-to-robot transformation matrix, T_{RC}, was computed by point-to-point rigid registration method [15].

In US calibration scanning procedure, the pose of calibration phantom was captured in optical tracking frame with the attached optical marker. By knowing the camera-to-robot transformation, the target point in optical tracking frame (p_C) thus was expressed in the robot frame as p_R. In this case, robot scanning can be programmed based on the target point. In free-hand calibration procedure, cross-wire phantom and sphere phantom require proficient skills to acquire enough images. The cross point needs to be viewed in the US image, and a wide scanning range covering different angles is indispensable. To meet the aforementioned requirements, the robotic scanning was characterised from free hand scanning and simplified as separate translation and rotation motions. The trajectories were optimized as motions along US probe axis and symmetric to eliminate bias. First, the US probe aligned with the cross point in vertical direction as initial position. Then, the probe rotated along the probe's X axis as shown in Fig. 4. Subsequently, it returned to its initial position and repeated the same movement along the Y axis and the Z axis. Then, the probe translated along X axis, Y axis and the Z axis respectively. During scanning, US images were recorded with corresponding 6 DoF poses simultaneously. After finishing all the motions, the probe returned to the initial position. The scanning time was recorded and data were processed. The attached marker must be detected once prior to actual scanning. Then the position of the phantom kept stationary during scanning. The rotation range was set as $\pm 20°$ for the cross-wire phantom while translation range was ± 2 mm to keep the target point in US plane. As the size of sphere phantom was larger than that of the cross-wire point, the rotation and translation range were increased to $\pm 30°$ and ± 5 mm to cover the whole geometry. Furthermore, it was important to set a proper scanning speed to reduce the influence of temporal offset between the raw images and corresponding recorded images (due to 30 Hz frame grabber). Nevertheless, a slow scanning speed cause longer scanning time. Thus, the scanning speed of the US probe tip was set as 2.5 mm/s for translation and 0.075 rad/s for rotation, respectively.

Different to the single point phantoms, calibration with Z phantom only required linear translation scanning thanks to the sophisticated phantom design. Thus, the robotic US scanning trajectory was optimized as a straight line while keeping the three layer "Z" shaped wires in all recorded images. During scanning, the US probe was initially placed close (10 mm) to the front phantom wall with the position control. Then, it moved 50 mm towards the back wall along the direction of line AB in Fig. 2 (c) and return to the front wall. During scanning, the US probe was perpendicular to the phantom bottom surface and kept the speed as 2.5 mm/s.

F. Evaluation

1) Calibration experiments: Since the scanning trajectories varied with phantom, the robotic scanning time for each phantom was recorded. After recording all data, the image processing time was also evaluated. The process time and the number of images were stored to evaluate the performance. The experimental testings were repeated three times for each calibration phantom and their performance results were shown in Table I. For each calculated calibration outcomes including transformation matrix (T_{MI}) and scaling factor matrix (T_s), they will be used in the 3D reconstruction validation.

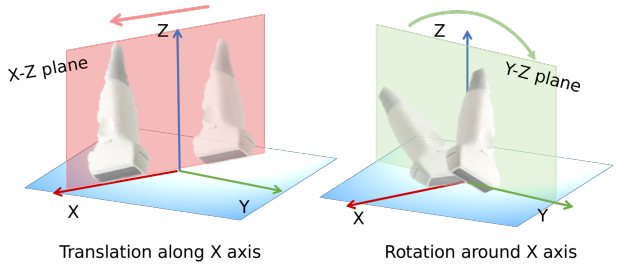

Fig. 4. An example of robotic US scanning motion. (Left) translation motion along x axis; (Right) rotation around x axis.

2) 3D reconstruction validation: The calibration results of different phantoms were evaluated by comparing the quality of 3D US reconstruction. A 3D printed mock-up model with known geometry was used for validation. The mock-up model consisted of various basic geometric features, such as cube, hemisphere, polyhedron and cone shown in Fig. 5. Before scanning, the mock-up model was placed in stationary in a water tank and assembled with an optical marker. The pose of mock-up model can be obtained and considered as the ground truth for quantitative evaluation. During robotic scanning, the US probe was kept perpendicular to the mock-up model bottom plane and moved along a predefined "S" shaped trajectory covering all area. After finishing the scanning, a similar image processing procedures were applied for 3D reconstruction to segment the outer contour mock-up model. For each phantom, the reconstructed point clouds were generated based on Eq. 1 with the calculated calibration outcomes. Then, the point clouds were assessed by calculating the distance to 3D position of the the ground truth, termed as 3D localization error. This error is used to show the actual displacement between the reconstructed point cloud and the target object. Besides, Iterative Closest Point (ICP) algorithm was used to register the generated point cloud with CAD model of the mock-up to obtain the 3D representation error that assesses the quality of reconstructed size and shape of the scanned model. The experimental test was repeated three times for those computed calibration matrices of each calibration phantom. Moreover, another 3D printed spine model (L3 to L5, generated from CT scan) was reconstructed to demonstrate feasibility of the three calibration methods to reconstruct a complex geometry. The root mean square error (RMSE), mean error and standard deviation (Std. Dev.) were

calculated with the aforementioned two models and present in Fig. 5 and Fig. 6.

III. Result

A. Robotic calibration experiments

The robotic scanning time were recorded during scanning, and the results were averaged among three repeated testings and rounded as integers, shown in the Table I. The robotic scanning time of the Z phantom was the fastest with 55 seconds. It took 97 and 108 seconds for the cross-wire phantom and the sphere phantom, respectively. Since the longer scanning process, the number of recorded US images were about 3000 for cross-wire phantom and sphere phantom, while only 1644 for Z phantom. The image segmentation time for each phantom was also different. The image processing time for the Z phantom was 0.04 second per image which is longer than the 0.02 seconds for the other phantoms.

TABLE I

CALIBRATION PERFORMANCE IN THREE PHANTOMS

procedure	items	cross-wire phantom	sphere phantom	Z phantom
robotic scanning	number of DoF	6	6	1
	translation range [mm]	[−2, 2]	[−5, 5]	[−50, 50]
	rotation range [°]	[−20, 20]	[−30, 30]	-
	time [s]	97	108	55
image processing	number of image	2906	3244	1644
	time [s]	70	76	64
	time per image [s]	0.02	0.02	0.04

B. 3D reconstruction

The reconstruction results based on the three calibration methods were shown in Fig. 5. The 3D representation RMSE of cross-wire phantom, sphere phantom and Z phantom were 1.06, 1.17 and 1.04 mm. It showed that these calibration methods possess geometries representation capability. Furthermore, to assess the 3D localization accuracy of the calibration results, the 3D reconstructed point clouds were compared with the ground truth. The RMSE of localization results were 1.54, 1.58 and 1.25 mm for cross-wire, sphere and Z phantom, respectively.

TABLE II

RESULTS OF RECONSTRUCTED SPINE MODEL (IN MILLIMETERS)

		cross-wire phantom	sphere phantom	Z phantom
3D Representation errors	RMSE	1.15	1.16	1.09
	Mean	1.36	1.70	1.21
	Std. Dev.	0.90	0.90	0.91
3D localization errors	RMSE	1.30	1.72	1.27
	Mean	1.71	2.98	1.62
	Std. Dev.	1.14	1.93	1.12

For the spine model, Table II shows the 3D representation and 3D localization errors. For Z phantom, the RMSE of 3D representation and localization were 1.09 and 1.27 mm respectively. It was noticed that these errors were smaller than those of cross-wire phantom and sphere phantom. Fig. 6 provides an example of the reconstructed point using Z phantom calibration parameters.

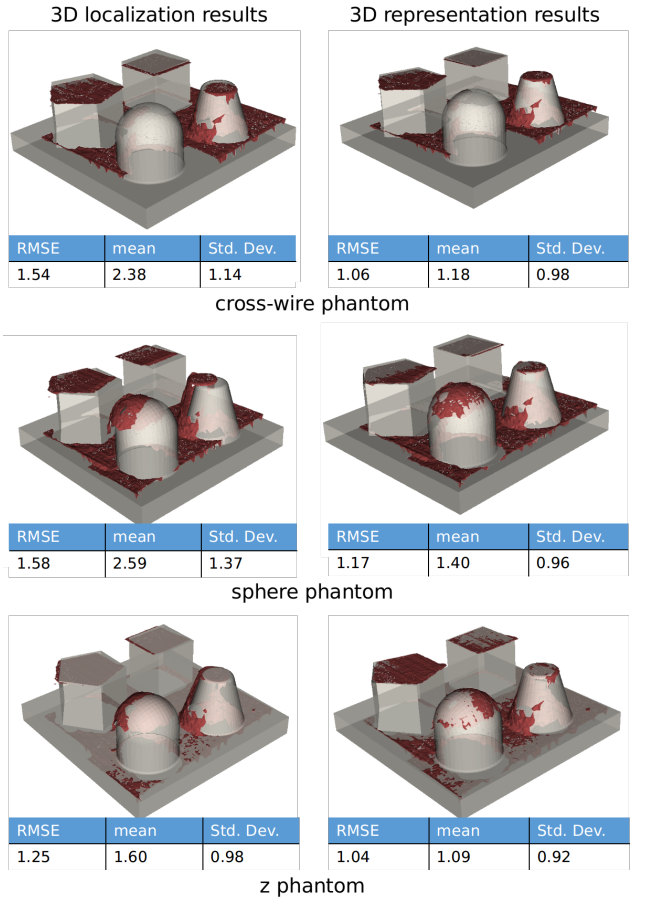

Fig. 5. Reconstruction point cloud(red) of custom designed mock-up model (gray) by using cross-wire phantom, sphere phantom and Z phantom. (Left) 3D localization error with ground truth; (Right) 3D representation error after ICP registration with CAD model. Results are given in millimeters.

IV. DISCUSSION

This paper analyzed three popular calibration phantoms in robotic US systems. Different aspects were investigated for a comprehensive comparison, ranging from phantom design to image processing. In the end, 3D US reconstruction was used as the criterion to assess the performance of each calibration method.

From design point of view, the cross-wire phantom and sphere phantom are easy to manufacture, since they only require few processes. Z phantom needs a precise manufacturing process to ensure the wires are located in the designed locations without displacement. For image processing, cross-wire phantom is scanned as a bright point in the US image. It is easy to distinguish, but subject to errors. Sphere phantom maps a semicircle in the US image. With least square method, the center of the sphere can be estimated accurately and used as the target point to solve the calibration equation.

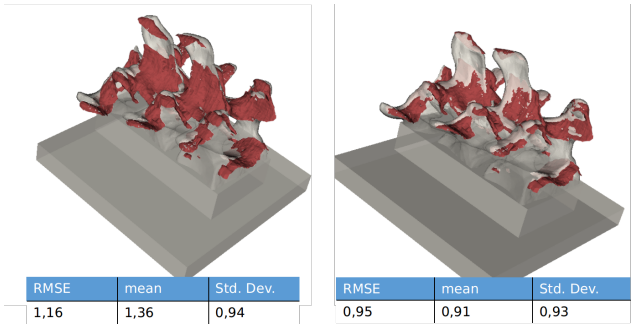

Fig. 6. An example of spine reconstruction (red) using Z phantom for calibration. (Left) 3D localization results with ground truth model (gray); (Right) 3D representation results after ICP registration with CAD model (gray). Results are given in millimeters.

The images acquired from Z phantom contain 9 clear Z-fiducial points. It takes more time than just segmenting one point for cross-wire. Thus the processing time of each image is 0.04 s for Z phantom which is larger than others (0.02 s). Previous researches reported the image process was up to hours [11]. In this paper, the total image processing time ranges from 64 to 76 seconds.

For robotic scanning trajectory, cross-wire phantom and sphere phantom require precise alignment between the US plane and target point, while Z phantom avoids this tedious procedure. The scanning requirement of Z phantom is to scan all Z-fiducial points in each image. Thus, the robotic scanning time of Z phantom is 55 second, which is shorter than the other two phantoms. The number of US images collected is related to the scanning time, the longer the time, the more images, and vice versa. The total calibration takes less than three minutes. It outperforms the calibration procedures in previous researches ranged from 10 to 35 min [9], [16]. The robotic scanning trajectories have great potential to be optimized in future. An efficient trajectory could reduce motion redundancy and shorten calibration time.

In the experimental part, the three proposed calibration approaches are validated by US reconstruction with 3D representation error and 3D localization error. From Fig. 5 and Table II, the 3D representation results illustrate that the reconstructed point clouds accurately outline the geometric features of mock-up model after ICP registration (RMSE: 0.95 mm). The results outperform the previous research [17], where their best reconstruction precision was 1.5 mm. Meanwhile, 3D localization results quantitatively show that the real pose and geometry feature of mock-up models could be precisely reconstructed in medical scenarios. Within included three phantoms, the RMSE of 3D representation and localization results are 1.04 and 1.25 mm by using the calibration parameters from Z phantom. They are smaller than the results derived by cross-wire phantom and sphere phantom. It indicates that the proposed robotic Z-phantom framework could obtain a fast and accurate US image calibration. This fact makes that Z phantom would be a good option for the researchers who target at high accuracy US image calibration.

V. CONCLUSION

This paper presents a quantitative comparison for robotic ultrasound image calibration. To conduct comparison, fully automatic robot-assisted US calibration frameworks are implemented for cross-wire phantom, sphere phantom and Z phantom. The proposed frameworks and comparative analysis of their performance would then provide guidance for future researchers in robotic US system.

REFERENCES

[1] C. Shi, X. Luo, J. Guo, Z. Najdovski, T. Fukuda, and H. Ren, "Three-Dimensional Intravascular Reconstruction Techniques Based on Intravascular Ultrasound: A Technical Review," IEEE J Biomed Health Inform, vol. 22, no. 3, pp. 806–817, 2018.

[2] P. M. B. Torres, J. Miguel Sanches, P. J. S. Goncalves, and J. M. M. Martins, "3D femur reconstruction using a robotized ultrasound probe," 4th IEEE RAS & EMBS International Conference on Biomedical Robotics and Biomechatronics, pp. 884-888, 2012.

[3] R. Li, K. Niu, D. Wu, and E. Vander Poorten, "A framework of realtime freehand ultrasound reconstruction based on deep learning for spine surgery," in 10th Conference on New Technologies for Computer and Robot Assisted Surgery, Location: Barcelona, Spain, 2020.

[4] Q. Huang, J. Lan, and X. Li, "Robotic Arm Based Automatic Ultrasound Scanning for Three-Dimensional Imaging," IEEE Transactions on Industrial Informatics, vol. 15, no. 2. pp. 1173–1182, 2019.

[5] Z. Jiang, M. Grimm, M. Zhou, Y. Hu, J. Esteban, and N. Navab, "Automatic Force-Based Probe Positioning for Precise Robotic Ultrasound Acquisition," IEEE Transactions on Industrial Electronics, vol. 68, no. 11, pp. 11200-11211, 2021.

[6] F. Rousseau, P. Hellier, M. M. J. Letteboer, W. J. Niessen, and C. Barillot, "Quantitative evaluation of three calibration methods for 3-D freehand ultrasound," IEEE Trans. Med. Imaging, vol. 25, no. 11, pp. 1492–1501, 2006.

[7] C. Kim, D. Chang, D. Petrisor, G. Chirikjian, M. Han, and D. Stoianovici, "Ultrasound probe and needle guide calibration for robotic ultrasound scanning and needle targeting," IEEE Trans. Biomed. Eng., vol. 60, no. 6, pp. 1728–1734, 2013.

[8] Q. Huang, B. Wu, J. Lan, and X. Li, "Fully Automatic Three-Dimensional Ultrasound Imaging Based on Conventional B-Scan," IEEE transactions on biomedical circuits and systems, vol. 12, no. 2, pp. 426–436, 2018.

[9] F. Aalamifar et al., "Robot-assisted automatic ultrasound calibration," International journal of computer assisted radiology and surgery, vol. 11, no. 10, pp. 1821–1829, 2016.

[10] Z. Jiang et al., "Autonomous Robotic Screening of Tubular Structures based only on Real-Time Ultrasound Imaging Feedback," IEEE Transactions on Industrial Electronics, 2021.

[11] P.-W. Hsu, R. W. Prager, A. H. Gee, and G. M. Treece, "Freehand 3D Ultrasound Calibration: A Review," Advanced Imaging in Biology and Medicine. pp. 47–84, 2009.

[12] E. Aertbelien and J. De Schutter, "eTaSL/eTC: A constraint-based task specification language and robot controller using expression graphs," proceedings of the 2014 IEEE/RSJ International Conference on Intelligent Robots and Systems, pp. 1540-1546, 2014.

[13] N. Pagoulatos, D. Haynor and Y. Kim, "A fast calibration method for 3D tracking of ultrasound images using a spatial localizer", Ultrasound in Medicine & Biology, vol. 27, no. 9, pp. 1219-1229, 2001.

[14] R. LI, K. Niu and E. Vander Poorten, "A Framework for Fast Automatic Robot Ultrasound Calibration", in International Symposium on Medical Robotics, Georgia Tech, Atlanta, US, 2021.

[15] K. Niu, J. Homminga, V. I. Sluiter, A. Sprengers, and N. Verdonschot, "Feasibility of a-mode ultrasound based intraoperative registration in computer-aided orthopedic surgery: a simulation and experimental study," Plos One, 2018.

[16] Y. Sato et al., "Image guidance of breast cancer surgery using 3-D ultrasound images and augmented reality visualization," IEEE Trans. Med. Imaging, vol. 17, no. 5, pp. 681–693, 1998.

[17] F. Cenni, S.-H. S. D. Monari, E. Aertbelien, K. Desloovere, and ¨H. Bruyninckx, "Efficient image based method using water-filled balloons for improving probe spatial calibration in 3d freehand ultrasonography," Ultrasonics journal, vol. 94, pp. 124–130, 2019.